



## 3D-QSAR Analysis of 2,4,5- and 2,3,4,5-Substituted Imidazoles as Potent and Nontoxic Modulators of P-Glycoprotein Mediated MDR

Ki H. Kim\*

*Department of Structural Biology, Abbott Laboratories, Abbott Park, IL 60064-6100, USA*

Received 13 December 2000; accepted 29 January 2001

**Abstract**—3D-Quantitative structure–activity relationships of 2,4,5- and 2,3,4,5-substituted imidazoles as a novel class of potent and nontoxic modulators of Pgp mediated MDR were investigated using CoMFA and COMSIA approaches. The best CoMFA model obtained from 46 imidazole analogues is a two-component model with the following statistics.  $R^2_{cv} = 0.643$ ,  $RMSE_{cv} = 0.360$  for the cross-validation, and  $R^2 = 0.767$ ,  $RMSE = 0.290$  for the fitted. The best COMSIA model obtained is also a two-component model with the following statistics.  $R^2_{cv} = 0.619$ ,  $RMSE_{cv} = 0.372$  for the cross-validation, and  $R^2 = 0.765$ ,  $RMSE = 0.292$  for the fitted. © 2001 Elsevier Science Ltd. All rights reserved.

### Introduction

Cancers treated with multiple anticancer drugs tend to develop cross-resistance to many other cytotoxic agents to which they had never been exposed. Such tumor cell resistance to chemotherapy is a major problem in the treatment of cancer. These phenomena, commonly referred to as multidrug resistance (MDR), are due to overexpression of an ATP-dependent transmembrane multidrug efflux pump P-glycoprotein (Pgp). Pgp actively extrudes structurally diverse compounds including not only anticancer drugs, but also therapeutic agents such as HIV-protease inhibitors.<sup>1,2</sup>

A number of noncytotoxic compounds known as MDR modulators or chemosensitizers sensitize resistant cells for the action of cytotoxic agents. They include calcium channel blockers, calmodulin antagonists, anthracyclines and Vinca alkaloid analogues, steroids and hormonal analogues, cyclosporins, cyclic peptides, and others.<sup>1–10</sup> Inhibition of drug transport could result from the blockage of specific substrate recognition, ATP hydrolysis, binding of ATP, coupling of ATP hydrolysis to translocation of the substrate, or regulating Pgp function by affecting posttranslational modifications.

Although many investigators studied various MDR modulators,<sup>1,3–20</sup> it still remains as one of the mysteries of this transport system how a single transport system can recognize so many different substrates.<sup>1</sup> Furthermore, very little quantitative structure–activity relationships (QSAR) are known about various MDR modulators.

Recently, Sarshar et al.<sup>9,10</sup> reported their studies on the trisubstituted imidazole analogues as a novel class of potent and nontoxic modulators of Pgp mediated MDR, which lead to the clinical candidate OC144-093. This manuscript describes the 3D-QSAR of these 2,4,5- and 2,3,4,5-substituted imidazoles using the technique of Comparative Molecular Field Analysis (CoMFA) and Comparative Molecular Similarity Indices Analysis (COMSIA).

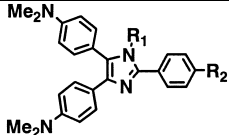
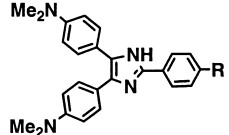
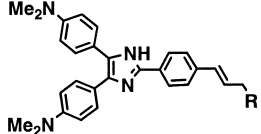
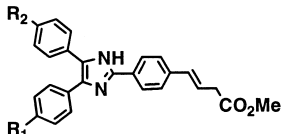
### Results and Discussions

Table 1 lists the compounds included in this study. The MDR modulating potency,  $ED_{50}$ , is the concentration of the compound that causes 50% inhibition of cell growth. In the correlation,  $\log 1/ED_{50}$  values were used. Therefore, the larger  $\log 1/ED_{50}$  value is, the more potent is the compound. Figure 1 shows all the compounds superimposed over the template compound (see Experimental).

The best CoMFA model obtained in this study from the 46 substituted imidazole analogues listed in Table 1 is a

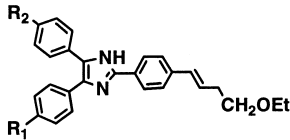
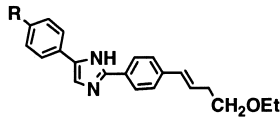
\*Corresponding author. Tel.: +1-847-937-5797; fax: +1-847-937-2625; e-mail: ki.h.kim@abbott.com

**Table 1.** Substituted imidazoles included in this study and their ED<sub>50</sub> values

No	Compound <sup>a</sup>	ED <sub>50</sub> , μM	Structure	
				
			R <sub>1</sub>	R <sub>2</sub>
47	Ref 1: 01	60.00	H	CO <sub>2</sub> H
1	Ref 1: 02	0.60	H	CO <sub>2</sub> Me
2	Ref 1: 03	2.00	<i>n</i> -Hexyl	CO <sub>2</sub> H
3	Ref 1: 04	6.00	<i>n</i> -Hexyl	CO <sub>2</sub> Me
48	Ref 1: 05	10.00	H	CH = CHCO <sub>2</sub> H
4	Ref 1: 06	0.30	H	CH = CHCO <sub>2</sub> Me
5	Ref 1: 07	5.00	H	OH
49	Ref 1: 08	1.00	Phenethyl	OH
6	Ref 1: 09	10.00	Phenethyl	CO <sub>2</sub> H
7	Ref 1: 10	20.00	Phenethyl	CH = CHCO <sub>2</sub> H
				
			R	
8	Ref 1: 15	1.00	CH <sub>2</sub> CH <sub>2</sub> CO <sub>2</sub> Me	
9	Ref 1: 16	0.60	CH = CHCN	
10	Ref 1: 17	0.13	CH = CHCN <sub>2</sub> OMe	
11	Ref 1: 18	0.08	CH = CHCH <sub>2</sub> OEt	
12	Ref 1: 19	0.30	CH <sub>2</sub> CH <sub>2</sub> CH <sub>2</sub> OMe	
13	Ref 1: 20	1.10	CH <sub>2</sub> CH <sub>2</sub> CH <sub>2</sub> CH <sub>2</sub> OMe	
14	Ref 1: 21	0.31		
				
			R	
15	Ref 1: 22	0.11	OBu	
16	Ref 1: 23	0.09	OCH <sub>2</sub> CH <sub>2</sub> OMe	
17	Ref 1: 24	0.30	OCH <sub>2</sub> Ph	
18	Ref 1: 25	0.45	OPh	
19	Ref 1: 26	0.88	OC(=O)NEt <sub>2</sub>	
20	Ref 1: 27	0.48	OC(=O)Bu	
21	Ref 1: 28	1.30	NMe <sub>2</sub>	
22	Ref 1: 29	0.96	<i>N</i> -Piperidine	
23	Ref 1: 30	0.32	<i>N</i> -Morpholine	
				
			R <sub>1</sub>	R <sub>2</sub>
24	Ref 2: 02	0.57	NEt <sub>2</sub>	NEt <sub>2</sub>
25	Ref 2: 03	0.37	Pyrrolidine	Pyrrolidine
50	Ref 2: 04	5.50	N(Allyl) <sub>2</sub>	N(Allyl) <sub>2</sub>
26	Ref 2: 05	0.13	NMe <sub>2</sub>	NHMe
27	Ref 2: 06	0.07	NEt <sub>2</sub>	NHMe
28	Ref 2: 07	0.18	NPr <sub>2</sub>	NHMe
51	Ref 2: 08	2.10	NBu <sub>2</sub>	NHMe
29	Ref 2: 09	0.59	NMe <sub>2</sub>	NH <sub>2</sub>
30	Ref 2: 10	0.31	NEt <sub>2</sub>	NH <sub>2</sub>
31	Ref 2: 11	0.20	NHMe	NHMe
32	Ref 2: 12	0.12	NH-i-Pr	NHMe

(continued on next page)

Table 1 (continued)

No	Compound <sup>a</sup>	ED <sub>50</sub> , $\mu$ M	Structure	
				
			R <sub>1</sub>	R <sub>2</sub>
33	Ref 2: 14	0.26	NEt <sub>2</sub>	NEt <sub>2</sub>
34	Ref 2: 15	0.22	N-Morpholine	N-Morpholine
35	Ref 2: 16	0.11	NHMe	NMe <sub>2</sub>
36	Ref 2: 17	0.06	NHMe	NEt <sub>2</sub>
37	Ref 2: 18	0.15	NHMe	N-Pyrrolidine
38	Ref 2: 19	0.05	NHMe	NH- <i>i</i> -Pr
39	Ref 2: 20	0.05	NHEt	NH- <i>i</i> -Pr
40	Ref 2: 21	0.16	F	NH- <i>i</i> -Pr
41	Ref 2: 22	0.05	NH- <i>i</i> -Pr	NH- <i>i</i> -Pr
				
			R	
42	Ref 2: 23	0.30	NEt <sub>2</sub>	
43	Ref 2: 24	0.28	NPr <sub>2</sub>	
44	Ref 2: 25	0.37	Morpholine	
45	Ref 2: 26	0.34	NH- <i>i</i> -Pr	
46	Ref 2: 27	0.25	NH- <i>i</i> -Bu	

<sup>a</sup>Ref 1 = reference 9 and Ref 2 = reference 10 in the reference section.

two-component model with the following statistics.  $R^2_{cv}=0.643$ ,  $RMSE_{cv}=0.360$  for the cross-validation, and  $R^2=0.767$ ,  $RMSE=0.290$  for the fitted. The steric portion of the influence of imidazole substituents for the MDR modulating potency described by this model is 52%, whereas the electrostatic portion is 48%. With a set of scrambled  $\log 1/ED_{50}$  values (see Experimental), no significant CoMFA model was obtained, and this supports that the CoMFA model described above was not obtained by chance: for one-component model,  $R^2_{cv}=-0.011$ ,  $RMSE_{cv}=0.671$  for the cross-validation, and  $R^2=0.359$ ,  $RMSE=0.534$  for the fitted.

Figure 2 shows the coefficient contour map of this model. In the contour map, the sterically favored

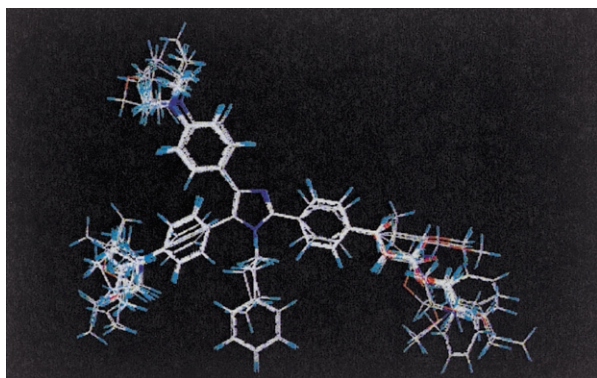


Figure 1. Superimposed position of the substituted imidazole analogues.

regions are shown in green, and the sterically disfavored regions are shown in yellow. The positive electrostatic contours are shown in blue, and the negative electrostatic contours are shown in red. Table 2 shows the observed and the calculated  $ED_{50}$  values from this two-component CoMFA model along their observed values. Figure 3a is a plot of the observed and the calculated  $\log 1/ED_{50}$  values from the CoMFA model. Five compounds showed a large deviation from this model (compounds 47–51 in Table 1) and were not included in this analysis (vide infra).

Although the CoMFA model has a moderate statistical quality, its contour plot provides useful information about the structure–activity relationships within this series. One of the two major sterically disfavored regions is where the N<sub>1</sub> imidazole ring substituent is (as in compounds 3, 4, and 8–10). Compounds 3 and 4 have an *n*-hexyl group, and compounds 8–10 have a phenethyl group at this position. The results indicate that such a large substituent at N<sub>1</sub>-position of the imidazole ring is not favored for improving MDR modulating potency. In addition, the N<sub>1</sub> substituent influences the orientation of the neighboring phenyl ring at the C<sub>5</sub>-position of the imidazole ring. A large substituent at N<sub>1</sub> position would force the neighboring phenyl ring into a different orientation from that of N<sub>1</sub>-unsubstituted analogue. This may not be beneficial for the potency. The other sterically disfavored region is around the *para*-substituent of the phenyl ring at C<sub>5</sub>-position of the imidazole ring. This sterically disfavored region (colored

in yellow) is positioned right next to a sterically favored region (colored in green). These two regions approximately correspond to the two alkyl positions of the *para*-*N,N*-dialkylaminophenyl group. The sterically favored and disfavored regions located next to each other in this region indicate that a secondary amine is preferred to a tertiary amine as a *para*-substituent. Such deteriorating effects of a tertiary alkyl substituent become greater as the size of the substituent becomes larger. This is consistent with the observation that among the tertiary

amine substituted analogues at both phenyl rings, the  $N(\text{allyl})_2$  substituted analogue (compound **26**) is less potent than the corresponding  $\text{NEt}_2$  analogue, and  $\text{NEt}_2$  is in turn less potent than the corresponding  $\text{NMe}_2$  analogue:  $N(\text{allyl})_2 < \text{NEt}_2 < \text{NMe}_2$ . Only a small region is seen as sterically favored on the *para*-substituted phenyl ring at  $C_4$ -position of the imidazole ring.

It is interesting to see that the sterically favored or disfavored regions are completely separated from the elec-

**Table 2.** Observed and calculated log  $1/\text{ED}_{50}$  values

No	Compound <sup>a</sup>	obs	Log $1/\text{ED}_{50}$					
			CoMFA		COMSIA		CoMFA	
			Calc <sup>b</sup>	Dev <sup>b</sup>	Calc <sup>c</sup>	Dev <sup>c</sup>	Calc <sup>d</sup>	Dev <sup>d</sup>
1	Ref 1: 02	6.222	6.058	0.163	6.891	−0.662	5.681	0.541
2	Ref 1: 03	5.699	5.164	0.535	5.905	−0.604	5.147	0.552
3	Ref 1: 04	5.222	5.253	−0.032	6.308	0.578	5.239	−0.017
4	Ref 1: 06	6.523	6.590	−0.067	5.149	0.550	6.339	0.183
5	Ref 1: 07	5.301	5.995	−0.694	5.217	−0.518	5.760	−0.459
6	Ref 1: 09	5.000	4.798	0.202	6.376	−0.489	4.844	0.156
7	Ref 1: 10	4.699	4.946	−0.247	6.713	0.442	5.052	−0.353
8	Ref 1: 15	6.000	6.017	−0.017	6.675	0.422	5.927	0.073
9	Ref 1: 16	6.222	6.062	0.160	6.911	−0.402	5.906	0.315
10	Ref 1: 17	6.886	6.472	0.414	6.688	0.358	6.423	0.463
11	Ref 1: 18	7.097	6.787	0.310	6.811	−0.343	6.756	0.341
12	Ref 1: 19	6.523	6.262	0.261	6.332	−0.315	6.153	0.370
13	Ref 1: 20	5.959	6.029	−0.070	5.908	0.314	5.950	0.008
14	Ref 1: 21	6.509	6.322	0.186	6.251	−0.293	6.256	0.253
15	Ref 1: 22	6.959	6.811	0.148	6.692	0.267	6.803	0.156
16	Ref 1: 23	7.046	6.659	0.387	7.070	−0.246	6.634	0.412
17	Ref 1: 24	6.523	6.832	−0.309	6.290	0.233	6.831	−0.308
18	Ref 1: 25	6.347	6.625	−0.278	6.657	0.229	6.616	−0.269
19	Ref 1: 26	6.056	6.283	−0.228	6.298	0.225	6.271	−0.215
20	Ref 1: 27	6.319	6.293	0.026	6.219	−0.219	6.259	0.060
21	Ref 1: 28	5.886	6.498	−0.612	7.097	0.204	6.454	−0.568
22	Ref 1: 29	6.018	6.566	−0.548	6.245	−0.189	6.542	−0.525
23	Ref 1: 30	6.495	6.591	−0.096	6.337	0.172	6.567	−0.072
24	Ref 2: 02	6.244	6.667	−0.423	7.139	0.162	6.385	−0.141
25	Ref 2: 03	6.432	6.570	−0.138	6.674	−0.151	6.410	0.022
26	Ref 2: 05	6.886	6.709	0.177	6.282	0.150	6.496	0.390
27	Ref 2: 06	7.155	6.803	0.352	6.772	0.149	6.569	0.586
28	Ref 2: 07	6.745	6.836	−0.091	7.152	0.149	6.543	0.202
29	Ref 2: 09	6.229	6.660	−0.431	7.086	0.136	6.474	−0.245
30	Ref 2: 10	6.509	6.752	−0.243	6.539	−0.107	6.536	−0.027
31	Ref 2: 11	6.699	6.633	0.066	6.215	0.104	6.483	0.216
32	Ref 2: 12	6.921	6.689	0.232	7.062	−0.103	6.550	0.371
33	Ref 2: 14	6.585	6.743	−0.158	6.327	−0.083	6.774	−0.189
34	Ref 2: 15	6.658	6.736	−0.078	6.879	−0.083	6.744	−0.087
35	Ref 2: 16	6.959	6.904	0.055	6.424	0.071	6.932	0.027
36	Ref 2: 17	7.222	6.998	0.224	6.666	−0.064	7.007	0.215
37	Ref 2: 18	6.824	6.916	−0.092	6.583	−0.060	6.955	−0.131
38	Ref 2: 19	7.301	6.924	0.377	4.945	0.055	6.975	0.326
39	Ref 2: 20	7.301	6.947	0.354	6.626	−0.041	6.973	0.328
40	Ref 2: 21	6.796	6.853	−0.057	5.257	−0.035	6.879	−0.083
41	Ref 2: 22	7.301	6.870	0.431	6.588	−0.035	6.905	0.396
42	Ref 2: 23	6.523	6.552	−0.030	6.188	0.034	6.583	−0.060
43	Ref 2: 24	6.553	6.601	−0.049	6.322	0.024	6.571	−0.018
44	Ref 2: 25	6.432	6.497	−0.065	6.723	0.022	6.515	−0.083
45	Ref 2: 26	6.469	6.569	−0.101	6.715	−0.016	6.611	−0.142
46	Ref 2: 27	6.602	6.508	0.094	6.650	0.007	6.557	0.045
47	Ref 1: 01	4.222	5.976 <sup>e</sup>	−1.754	5.818 <sup>e</sup>	−1.596	5.540	−1.318
48	Ref 1: 05	5.000	6.351 <sup>c</sup>	−1.351	6.158 <sup>c</sup>	−1.158	6.029	−1.029
49	Ref 1: 08	6.000	4.834 <sup>e</sup>	1.166	5.096 <sup>c</sup>	0.904	4.966	1.034
50	Ref 2: 04	5.260	6.645 <sup>c</sup>	−1.385	6.320 <sup>c</sup>	−1.060	6.168	−0.908
51	Ref 2: 08	5.678	6.822 <sup>e</sup>	−1.144	6.721 <sup>c</sup>	−1.043	6.472	−0.795

<sup>a</sup>Ref 1 = reference 9 and Ref 2 = reference 10 in the reference section.

<sup>b</sup>Calculated from the CoMFA model ( $n=46$ ,  $L=2$ ).

<sup>c</sup>Calculated from the COMSIA model ( $n=46$ ,  $L=2$ ).

<sup>d</sup>Calculated from the CoMFA model ( $n=51$ ,  $L=2$ ).

<sup>e</sup>Not used in the analysis.

trostatically positive or negative regions in Figure 2. The positive or negative electrostatic contour regions are located where the cinnamic acid (e.g., **7**, **48**) or ester (e.g., **4**) moiety is present in some molecules at the para-position of the phenyl ring at the C<sub>2</sub>-site of the imidazole ring. Since the core molecular area as indicated by the template molecule (Fig. 6) does not vary, it is not surprising to see no contours around this region.

Sometimes an improved 3D-QSAR model can be obtained with COMSIA, another 3D-QSAR approach.<sup>21,22</sup> However, very similar results were obtained with this approach with the present set of data. The best COMSIA model obtained from 46 imidazole analogues was a two-component model with the following statistics.  $R^2_{cv} = 0.619$ ,  $RMSE_{cv} = 0.372$  for the cross-

validation, and  $R^2 = 0.765$ ,  $RMSE = 0.292$  for the fitted. With a scrambled log 1/ED<sub>50</sub> values (see Experimental), no significant COMSIA model was obtained, and this supports that the COMSIA model described above was not obtained by chance: for one-component model,  $R^2_{cv} = -0.059$ ,  $RMSE_{cv} = 0.686$  for the cross-validation, and  $R^2 = 0.333$ ,  $RMSE = 0.545$  for the fitted. Although the steric and electrostatic, donor and acceptor, and hydrophobic fields were initially used, only the first four fields were found to be important. The hydrophobic fields did not significantly contribute to the correlation.

Table 1 lists the calculated log ED<sub>50</sub> values from the two-component COMSIA model. Figure 4 shows the COMSIA coefficient contour map. The sterically favored regions are shown in green, and the sterically

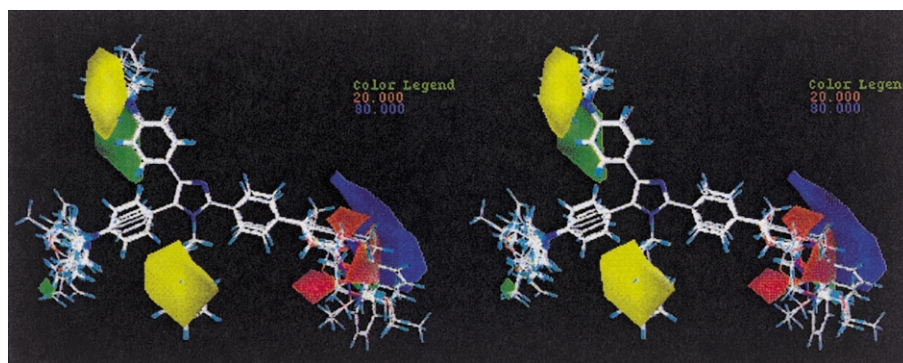


**Figure 2.** CoMFA coefficient contour map from  $n=46$ . The sterically favoured regions are shown in green, and the sterically disfavoured regions are shown in yellow. The positive electrostatic contours are shown in blue, and the negative electrostatic contours are shown in red.

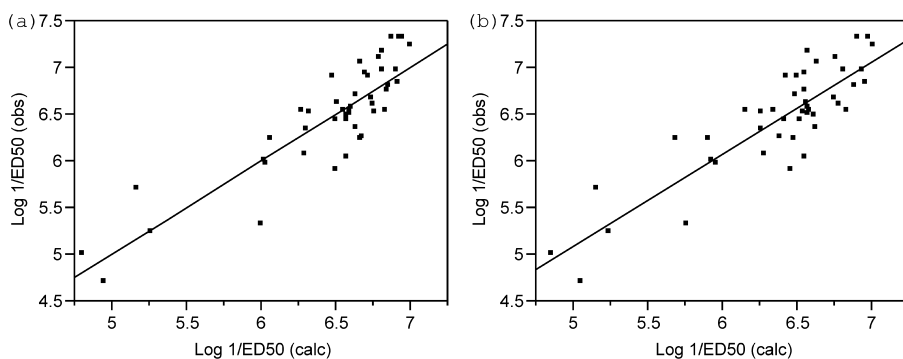


**Figure 3.** Plot of the observed versus calculated log 1/ED<sub>50</sub> values using the two component CoMFA model (a) and COMSIA model (b).

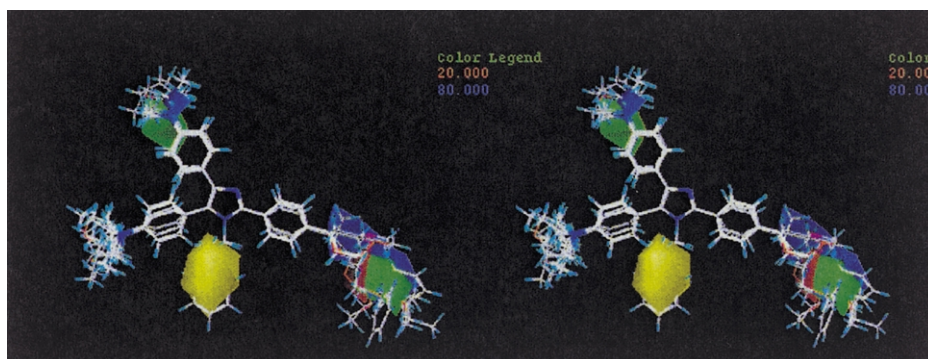


**Figure 4.** COMSIA coefficient contour map from  $n=46$ . The sterically favored regions are shown in green, and the sterically disfavoured regions are shown in yellow. The positive electrostatic contours are shown in blue, and the negative electrostatic contours are shown in red.



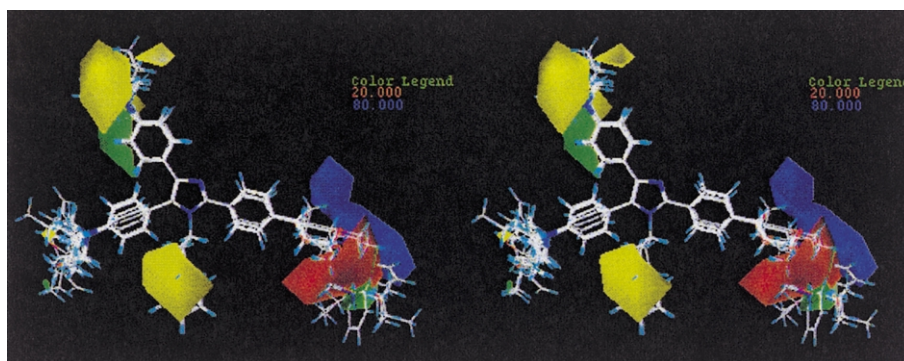


**Figure 5.** CoMFA coefficient contour map from  $n=51$ . The sterically favored regions are shown in green, and the sterically disfavored regions are shown in yellow. The positive electrostatic contours are shown in blue, and the negative electrostatic contours are shown in red.

disfavored regions are shown in yellow. The positive electrostatic contours are shown in blue, and the negative electrostatic contours are shown in red. CoMFA contours shown in Figure 3 and the COMSIA contours shown in Figure 4 contain very similar information about the steric and electrostatic influences on MDR modulating potency. However, some differences are noted as well. The first is the sterically disfavored region around the *para*-substituent of the phenyl ring at C<sub>4</sub>-position of the imidazole ring. The CoMFA contour indicates that there is a sterically disfavored region around the phenyl substituent, whereas the COMSIA does not show this. The second is that COMSIA contour map shows a sterically favored region around the phenyl substituent at C<sub>2</sub>-position of the imidazole ring, whereas in CoMFA contour map it is almost negligible. This is where the cinnamic acid, ester, or alcohol moiety is present in some molecules. It is interesting to note that this sterically favored region shown in COMSIA model can be also seen in the CoMFA contour map (Fig. 5) of the model derived from all 51 compounds. Therefore, this second sterically favored region may also be important for the MDR modulating potency. This result demonstrates one benefit of investing 3D-QSAR using more than one approach. Figure 3b is the plot between the observed and calculated  $\log 1/ED_{50}$  values from the two-component COMSIA model. The ranking of the calculated potency for compound **41**, the clinical candidate, is 5th by the CoMFA model, whereas it is 24th by the COMSIA model. In this regard, the CoMFA model appears to be somewhat preferred to the corresponding COMSIA model.

Five compounds showed a large deviation from the two-component CoMFA model. They are compounds **47–51** in Table 1. Compound **49** was found to have higher than expected potency. Although this compound is expected to be weak ( $\sim 13 \mu\text{M}$ ), the observed potency is about 10 times more potent ( $1 \mu\text{M}$ ) than the expected potency from the CoMFA model. The other four com-

pounds showed weaker than expected potency by the CoMFA model. The reason for the poor fit of these compounds is not clear at this point. All five compounds show similar deviation from the corresponding two-component COMSIA model.

Figure 4 shows the coefficient contours from the two-component model derived from all 51 compounds. Both the steric and electrostatic contours are essentially identical to those in Figure 2 except the *para*-substituent region of C<sub>2</sub>-position of the imidazole ring. Inclusion or exclusion of the five compounds does not significantly alter the 3D-QSAR information provided by the earlier CoMFA model obtained from just 46 compounds.

There are at least two other compounds (compounds **38** and **39**) that have an identical  $ED_{50}$  value as OC144-093 (compound **41**), although the original authors selected OC144-093 as the clinical candidate. However, compound **41** yielded the best pharmacokinetic properties with a half life of 2.79 h and 41% bioavailability in dogs when administered 5 mg/kg, iv and 10 mg/kg, po.

The CoMFA and COMSIA models obtained in this study are, to our knowledge, the first 3D-QSAR reported from MDR modulators as well as substituted imidazole analogues. It is hoped that the QSAR information reported here and from other modulators would be helpful to solve the mysteries of Pgp transport system in not too distant future.

## Summary

3D-Quantitative structure–activity relationships of 2,4,5- and 2,3,4,5-substituted imidazoles as a novel class of potent and nontoxic modulators of Pgp mediated MDR were investigated using the CoMFA and the COMSIA methods. A two-component model with a similar statistical quality was obtained by either the CoMFA or the COMSIA approach.

## Experimental

The assays<sup>9,10</sup> were carried out in the presence of vinblastine and the corresponding 2,4,5- and 2,3,4,5-sub-



**Figure 6.** Template molecule used for superposition.

stituted imidazoles compound (0.01–50  $\mu$ M): Verapamil was used as the reference standard. The cell line used was CEM/VLB1000 human lymphoma cell line that overexpresses Pgp.

The molecular modeling of the compounds was done using the molecular modeling package Sybyl (Version 6.6) of Tripos, Inc. The initial geometry of the compounds was built by the CONCORD program.<sup>23</sup> These initial geometries were then optimized using the Sybyl minimization procedures with the following options: method = Powell, initial optimization = simplex, termination = gradient, 0.05 kcal/mol, max iterations = 100, and all others in the default setting of Sybyl 6.6 version.

Although the majority of the compounds modeled initially had a similar conformation of the two or three phenyl ring torsion angles with respect to the imidazole ring, several compounds had one or more phenyl rings rotated to an opposite direction. These torsion angles were manually rotated before the geometry minimization, so that all the analogues had a consistent ring and side chain orientation. Several compounds have somewhat different torsion angles for the phenyl ring at C4-position of the imidazole ring because of the steric repulsions between the neighboring groups when N1 of the imidazole ring was substituted as in compounds **3**, **4**, **8**, **9**, and **10**. When the *para*-substituents on the two phenyl rings were not the same, their conformation was chosen in such a way that a bulkier group was orientated in the same direction (substituted phenyl position at C5-position of the imidazole ring).

The point charges were calculated by the Gasteiger–Hückel method implemented in Sybyl. Overlapping the atomic position of the template molecule shown in Figure 6 did superposition of the entire molecules. Figure 1 shows all the compounds superimposed over the template compound. Standard CoMFA Csp3 probe atom with +1 charge was used with 2 angstrom grid size for the steric and electrostatic field calculations. The grid box used was created automatically by the program with X = –16.79 to 16.18, Y = –11.81 to 15.12, and Z = –11.63 to 9.89. For the scrambling log 1/ED<sub>50</sub> values, the compound names and log 1/ED<sub>50</sub> value columns were first sorted independently. Then, the sorted log 1/ED<sub>50</sub> values were assigned to the sorted compounds starting from the second compound. (It was started from the second compound because the first compound was the same compound in both cases).

For the COMSIA field calculations, the steric and electrostatic, the donor and acceptor, and the hydrophobic

fields were calculated separately with the default attenuation factor (0.3) for the same grid box and size used in CoMFA.

## References

1. Ambudkar, S. V.; Dey, S.; Hrycyna, C. A.; Ramachandra, M.; Pastan, I.; Gottesman, M. M. *Annu. Rev. Pharmacol. Toxicol.* **1999**, 39, 361.
2. Ford, J. M.; Hait, W. N. *Pharmacol. Rev.* **1990**, 42, 155.
3. Boger, D.; Boyce, C. W.; Labroli, M. A.; Sehon, C. A.; Jin, Q. *J. Am. Chem. Soc.* **1999**, 121, 54.
4. Boger, D.; Soenen, D. R.; Boyce, C. W.; Hedrick, M. P.; Jin, Q. *J. Org. Chem.* **2000**, 65, 2479.
5. Gelmi, M. L.; Mottadelli, S.; Pocar, D.; Riva, A.; Bombardelli, E.; Vincenzo, R. D.; Scambia, G. *J. Med. Chem.* **1999**, 42, 11953.
6. Lampidis, T. J.; Kolonias, D.; Podona, T.; Israel, M.; Safa, A. R.; Lothstein, L.; Savaraj, N.; Tapiero, H.; Priebe, W. *Biochem.* **1997**, 36, 2679.
7. Depew, K. M.; Marsden, S. P.; Zatorska, D.; Zatorski, A.; Bornmann, W. G.; Danishefsky, S. J. *J. Am. Chem. Soc.* **1999**, 121, 11953.
8. Chiba, P.; Burghofer, S.; Richter, E.; Tell, B.; Moser, A.; Ecker, G. *J. Med. Chem.* **1995**, 38, 2789.
9. Sarshar, S.; Zhang, C.; Moran, E. J.; Krane, S.; Rodarte, J. C.; Benbatoul, K. D.; Dixon, R.; Mjalli, A. M. M. *Bioorg. Med. Chem. Lett.* **2000**, 10, 2599.
10. Zhang, C.; Sarshar, S.; Moran, E. J.; Krane, S.; Rodarte, J. C.; Benbatoul, K. D.; Dixon, R.; Mjalli, A. M. M. *Bioorg. Med. Chem. Lett.* **2000**, 10, 2603.
11. Bakken, G. A.; Jurs, P. C. *J. Med. Chem.* **2000**, 43, 4534.
12. Seelig, A. E. *J. Biochem.* **1998**, 251, 252.
13. Sawanishi, H.; Sawanishi, H.; Wakusawa, S.; Murakami, R.; Miyamoto, K. *Chem. Pharm. Bull.* **1994**, 42, 1459.
14. Gutknecht, J.; Tosteson, D. C. *J. Gen. Physiol.* **1970**, 55, R818.
15. Selassie, C. D.; Hansch, C.; Khwajia, T. A. *J. Med. Chem.* **1990**, 33, 1914.
16. Chen, Y.-N.; Mickley, L. A.; Schwartz, A. M.; Acton, E. M.; Hwang, J.; Fojo, A. T. *J. Biol. Chem.* **1990**, 265, 10073.
17. Ecker, G.; Chiba, P.; Hitzler, M.; Schmid, D.; Visser, K.; Cordes, H. P.; Csollei, J.; Seydel, J. K.; Schaper, K.-J. *J. Med. Chem.* **1996**, 39, 4767.
18. Goldstein, L. J. *Curr. Probl. Cancer* **1995**, 19, 65.
19. Ford, J. M. *Eur. J. Cancer* **1996**, 32A, 991.
20. Klopman, G.; Shi, L. M.; Ramu, A. *Mol. Pharmacol.* **1997**, 52, 323.
21. Klebe, G.; Abraham, U.; Mietzner, T. *J. Med. Chem.* **1994**, 37, 4130.
22. Klebe, G. *Perspect. Drug Discovery Design* **1998**, 12, 87.
23. Rusinko, A., III; Sheridan, R. P.; Nilakantan, R.; Haraki, K. S.; Bauman, N.; Venkataraghavan, R. *J. Chem. Inf. Comput. Sci.* **1989**, 29, 251.